SUPPLEMENTARY INFORMATION: Deterministic Field-Free Skyrmion Nucleation at a Nano-Engineered Injector Device

Simone Finizio,[1,*] Katharina Zeissler,[2] Sebastian Wintz,[1,3] Sina Mayr,[1,4] Teresa Weßels,[5] Alexandra J. Huxtable,[2] Gavin Burnell,[2] Christopher H. Marrows,[2] and Jörg Raabe[1]

[1]*Swiss Light Source, Paul Scherrer Institut, 5232 Villigen PSI, Switzerland*

[2]*School of Physics and Astronomy, University of Leeds, Leeds LS2 9JT, United Kingdom*

[3]*Institute of Ion Beam Physics and Materials Research, Helmholtz-Zentrum Dresden-Rossendorf, 01328 Dresden, Germany*

[4]*Department of Materials, Laboratory for Mesoscopic Systems, ETH Zürich, 8093 Zürich, Switzerland*

[5]*Ernst Ruska-Centre for Microscopy and Spectroscopy with Electrons and Peter Grünberg Institute 5, Forschungszentrum Jülich, 52425 Jülich, Germany*

(Dated: September 17, 2019)

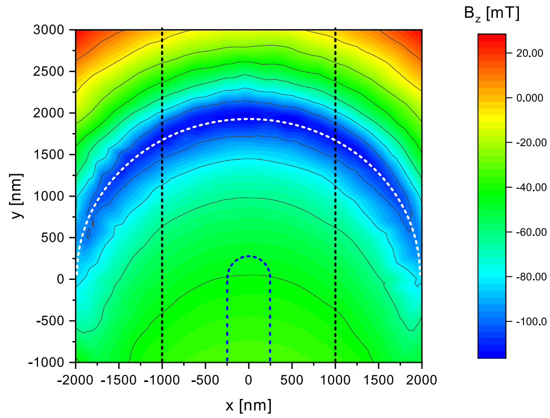

Figure S1. Finite element simulation of the out-of-plane component of the magnetic field generated by the injection of a 350 mA current pulse across the Ω-shaped coil. The white dashed line indicates the edge of the Ω-shaped coil, the black dashed lines indicate the edges of the microwire, and the blue dashed line marks the edge of the skyrmion injector.

Simulation of the magnetic field generated by the Ω-shaped microcoil

The spatial distribution of the magnetic field generated by the Ω-shaped microcoil when annihilating the magnetic skyrmion was simulated with the commercial finite element multiphysics simulation suite ANSYS (see the Methods section for more details). The results of the simulations are shown in Fig. S1.

Simulation of the current density distribution in and around the skyrmion injector

The spatial distribution of the current density in the Pt/$Co_{68}B_{32}$/Ir microstructured wire when injecting a current pulse across the skyrmion injector was simulated once again using the commercial finite element multiphysics simulation suite ANSYS (see the Methods section for more details). The results of the simulations are shown in Fig. S2. It is possible to observe that a hot spot in the current density can be found at the tip of the skyrmion injector. In this point, a current density about a factor 3 higher than in the uniform section of the microwire can be observed.

It is also possible to observe that the elongated shape of the magnetic skyrmions nucleated in the time-resolved experiments presented in Figs. 4 and 5 of the main manuscript resembles the shape of the hot spot in the current density at the tip of the injector structure, suggesting

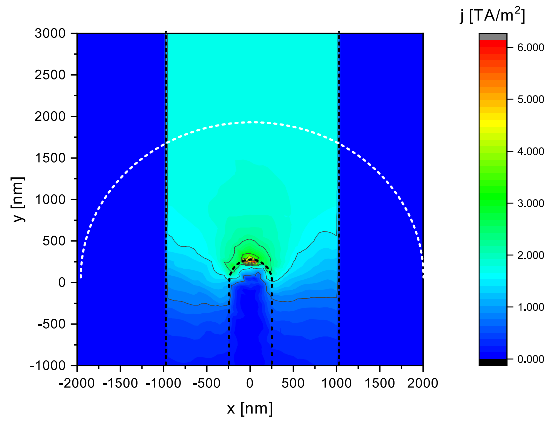

Figure S2. Finite element simulation of the spatial distribution of the current density in the Pt/$Co_{68}B_{32}$/Ir microwire when injecting a current pulse across the skyrmion injector. The white dashed line indicates the edge of the Ω-shaped coil, while the black dashed lines indicate the edges of the microwire and of the skyrmion injector.

that the shape of the nucleated skyrmion could be controlled by tailoring the distribution of the injected current density at the tip of the skyrmion injector.

Measurement of the dynamical temperature variation in the Pt/$Co_{68}B_{32}$/Ir multilayer stack

The injection of a current pulse into the microwire causes its heating due to Ohmic losses. To estimate the dynamical variation of the temperature of the Pt/$Co_{68}B_{32}$/Ir multilayer stack in the region where the skyrmion nucleation occurs, we determined the time-resolved variation of the saturation magnetization M_s of the Pt/$Co_{68}B_{32}$/Ir multilayer stack by measuring the variation in contrast in the uniformly magnetized region of the sample (see inset of Fig. S3). This measurement was normalized to the variation in magnetic contrast recorded in the region where the skyrmion is nucleated (where the magnetization switches completely). Under the assumption that the Pt/$Co_{68}B_{32}$/Ir multilayer stack remains perpendicularly magnetized during the injection of the current pulse, the time-resolved variation of M_s calculated from the time-resolved images is shown in Fig. S3.

The time-resolved variation of the sample temperature was then determined by comparing the time-resolved variation of M_s with the static variation of M_s in the Pt/$Co_{68}B_{32}$/Ir multilayer stack as a function of the temperature measured by SQUID-VSM, shown in Fig.

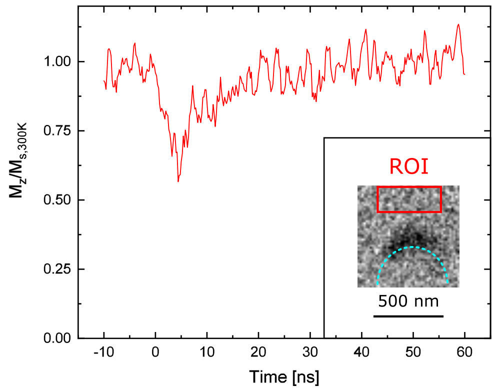

Figure S3. Time-resolved variation of the saturation magnetization (normalized to the saturation magnetization at room temperature) of the Pt/$Co_{68}B_{32}$/Ir multilayer stack in the region surrounding the skyrmion injector (area marked by ROI in the inset).

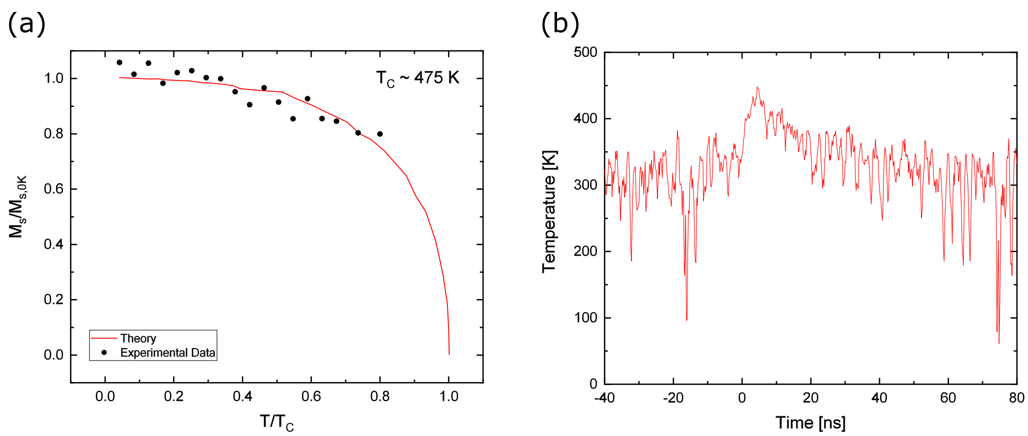

Figure S4. Comparison of the time-resolved variation in M_s with the static dependence of M_s as a function of the temperature. (a) Static dependence of M_s as a function of the temperature, fitted to the expected dependence of $M_s(T)$. (b) Calculated time-resolved temperature of the Pt/$Co_{68}B_{32}$/Ir multilayer stack in the region surrounding the skyrmion injector.

S4(a), where a Curie temperature of about 475 K could be estimated for the Pt/$Co_{68}B_{32}$/Ir. The result of such calculation is shown in Fig. S4(b), where it is possible to observe that the maximum temperature after the injection of a 5 ns wide current pulse with a peak current density of 1.4×10^{12} Am^{-2} is of about 420-440 K, which approaches, but does not exceed the Curie temperature of the Pt/$Co_{68}B_{32}$/Ir stack.

To verify that the region of interest we show in the inset of Fig. S3 allows us to obtain a reasonable estimation of the temperature of the Pt/$Co_{68}B_{32}$/Ir microwire, we performed

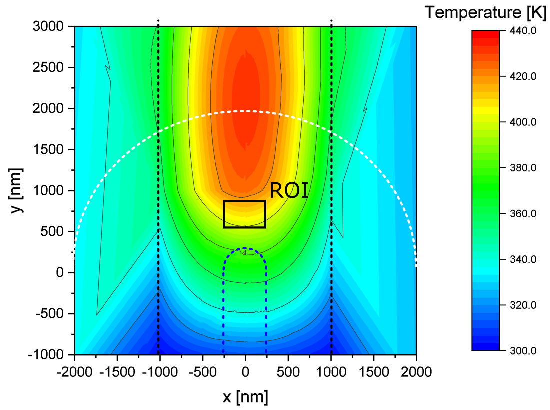

Figure S5. Heatmap showing the simulated distribution of the temperature of the Pt/$Co_{68}B_{32}$/Ir microwire after a 5ns long current pulse simulating the experiments reported in the main manuscript. The maximum of the temperature (440 K) occurs at the center of the microwire, away from the Cu contacts, which also act as heat sinks. The white dashed line indicates the edge of the Ω-shaped coil, the black dashed lines indicate the edges of the microwire, and the blue dashed line indicates the edge of the skyrmion injector. The ROI used for the experimental determination of the temperature of the microwire is shown in the image as well, showing that the temperature recorded there overestimates the temperature of the microwire in the region where the magnetic skyrmion is nucleated.

finite element simulations of the temperature in the microwire using the commercial multiphysics finite element simulation software ANSYS. From the results of the simulations shown in Fig. S5, it is possible to observe that the maximum in the temperature is not located at the tip of the injector structure, but rather at the center of the microwire. This is due to the fact that, despite the presence of an area directly in front of the injector where the current density is about a factor three higher than in the rest of the microwire, most of the energy of the pulse is dissipated in the section of the microwire exhibiting a uniform distribution of the current density. Furthermore, the region around the injector structure can, thanks to the presence of the thick Cu injector, dissipate the heat generated by the injected current more efficiently than the central section of the microwire, providing an additional justification for the results of the temperature simulations. The simulations also allow us to conclude that the temperature in the region of interest marked in the inset of Fig. S3 is slightly overestimating the temperature in the skyrmion nucleation region.

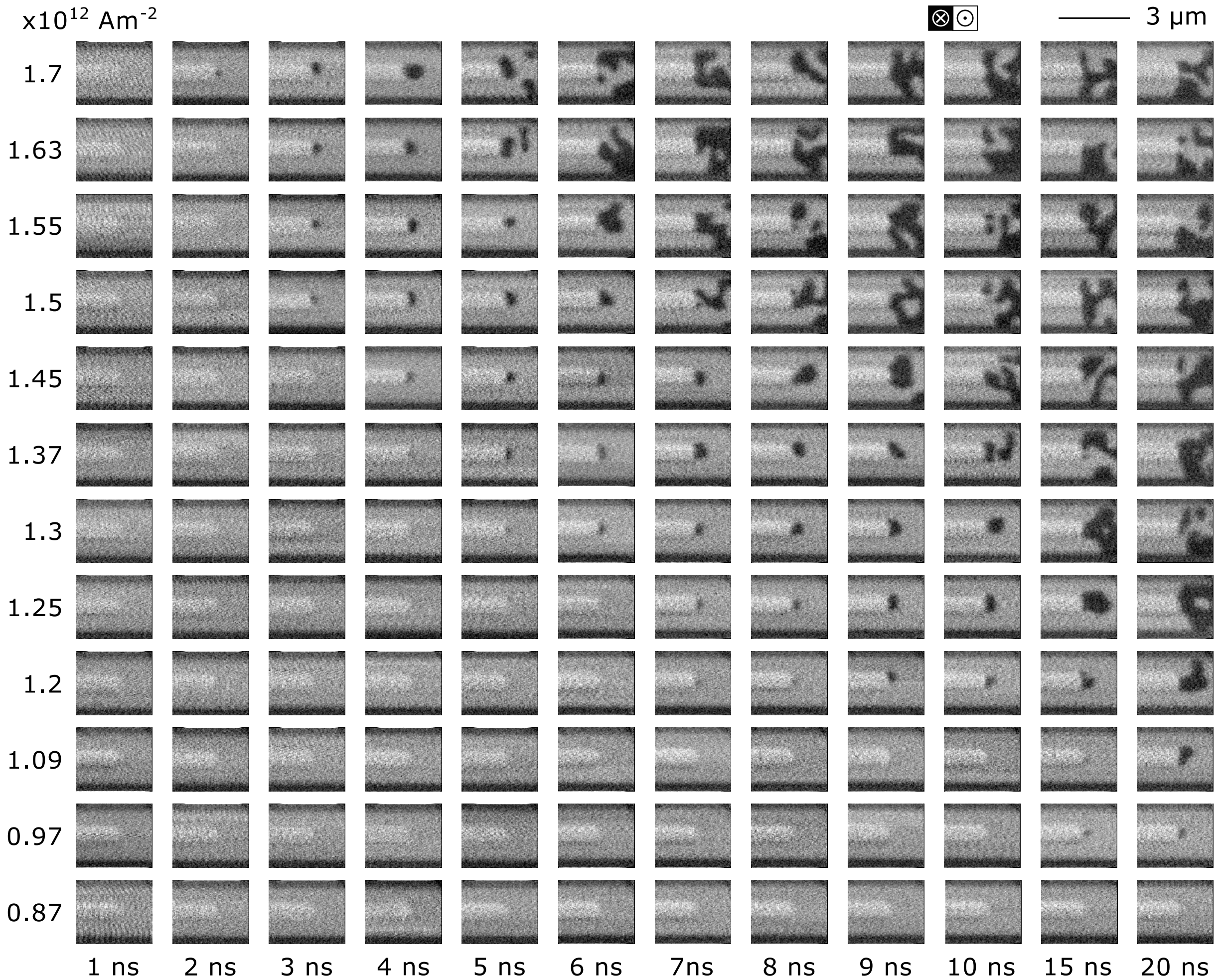

Figure S6. Quasi-static XMCD-STXM images of the skyrmion nucleation process as a function of pulse width and of the injected current density.

XMCD-STXM images of the skyrmion nucleation process

In this section, the quasi-static XMCD-STXM images employed to obtain the results shown in Figs. 2 and 3 of the main manuscript are shown. A multidomain state was identified by the presence of either multiple domains in the field of view of the image, or by the presence of magnetic domains in contact with the edges of the microwire.

Influence of the pulse characteristics on the skyrmion area

Here, the influence of the specifications of the current pulse injected in the $Pt/Co_{68}B_{32}/Ir$ microwire on the area of the skyrmions nucleated by the pulse is shown. As described in

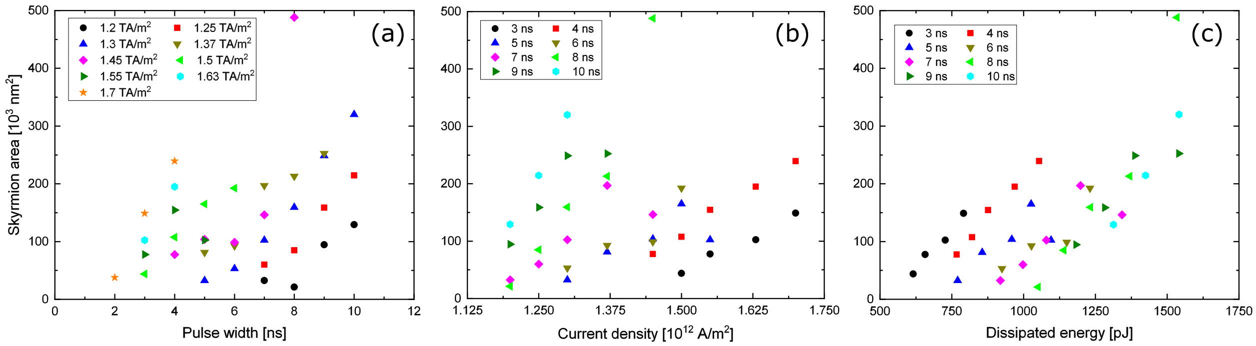

Figure S7. Dependence of the area of the magnetic skyrmions nucleated with a current pulse with respect to (a) the width of the current pulse (under equal current density), (b) the current density injected by the pulse (under equal pulse width), and on (c) the energy dissipated by the pulse (under equal pulse width).

the main manuscript, the increase of either the width or the current density of the injected pulse leads to an increase in the area of the nucleated magnetic skyrmion. A roughly linear dependence with either the width or the current density can be observed.

Zero-field stability of skyrmions

The zero-field stability of the magnetic skyrmions in the Pt/$Co_{68}B_{32}$/Ir multilayer stack reported here was also observed in micromagnetic simulations of the PMA stack. To simulate the stack, a simulation grid of $1 \times 1 \times 0.1$ nm^3 was employed. Three magnetic layers of 0.8 nm thickness separated by nonmagnetic layers of 1 nm thickness were simulated.

An example of the results of such simulations is shown in Fig. S8, where a magnetic skyrmion with a diameter of about 150 nm could be stabilized in absence of externally applied magnetic fields.

* Corresponding Author: simone.finizio@psi.ch

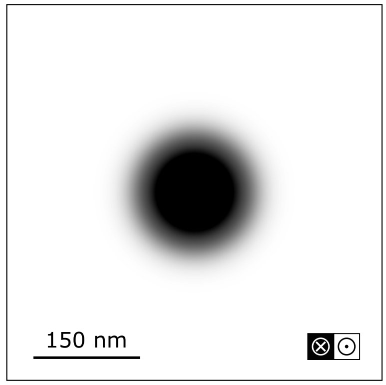

Figure S8. Micromagnetic simulation of a continuous film of Pt/$Co_{68}B_{32}$/Ir, where it is possible to observe that an isolated magnetic skyrmion of about 150 nm diameter can be stabilized in absence of externally applied magnetic fields. The black/white legend indicates the direction of the magnetization in the image.